Journal of Classical Analysis
Volume 3, Number 1 (2013), 1–15
doi:10.7153/jca-03-01

ASYMPTOTICS OF THE GAUSS HYPERGEOMETRIC FUNCTION WITH LARGE PARAMETERS, II

R. B. PARIS

Abstract. We obtain asymptotic expansions by application of the method of steepest descents for the Gauss hypergeometric function

$$F(a+\varepsilon_1\lambda, b+\varepsilon_2\lambda; c+\lambda; z)$$

as $|\lambda|\to\infty$ when $0<\varepsilon_1<1$ and $\varepsilon_1>1$ where, without loss of generality, it is supposed that $\varepsilon_1\leqslant\varepsilon_2$. The resulting expansions are of Poincaré type and break down in the neighbourhood of certain critical points in the z-plane. Numerical results illustrating the accuracy of the different expansions are given.

1. Introduction

This is the continuation of [2] on the asymptotic expansion of the Gauss hypergeometric function

$$F\left(\begin{matrix}a+\varepsilon_1\lambda, b+\varepsilon_2\lambda\\ c+\varepsilon_3\lambda\end{matrix};z\right) \tag{1.1}$$

for large complex values of λ when the parameters ε_j are finite. It was shown that it is sufficient to consider just three basic types of hypergeometric function corresponding to the parameter sets $(\varepsilon,0,1)$ (Type A), $(\varepsilon,-1,0)$ (Type B) and $(\varepsilon_1,\varepsilon_2,1)$ (Type C). The expansion of (1.1) for large $|\lambda|$ corresponding to Types A and B was discussed in [2]. Here we shall consider the expansion of functions of Type C.

It is clear that, by a straightforward scaling of λ, it is possible to take $\varepsilon_3=1$ without loss of generality and so consider the function

$$F_3(\lambda;z)\equiv F\left(\begin{matrix}a+\varepsilon_1\lambda, b+\varepsilon_2\lambda\\ c+\lambda\end{matrix};z\right). \tag{1.2}$$

In addition, from the symmetry of $F(a,b;c;z)$ in the numerator parameters a and b, it is sufficient to take $\varepsilon_1\leqslant\varepsilon_2$. The treatment of this function then divides itself into two cases: (i) $0<\varepsilon_1<1$ and (ii) $\varepsilon_1>1$. The case $\varepsilon_1=1$ can be excluded from our consideration, since $F_3(\lambda;z)$ reduces to a function of Type B by application of transformation (T1) in [2, §2]; if, in addition $\varepsilon_2=1$, the transformation (T1) can be applied again to reduce $F_3(\lambda;z)$ to $F(c-a,c-b;c+\lambda;z)$ with a single large parameter in the denominator, for which the expansion is well known [1, p. 397].

Mathematics subject classification (2010): Primary 33C05, 34E05, 41A60.
Keywords and phrases: Hypergeometric functions, asymptotic expansion, large parameters.

Paper JCA-03-01

Although some of the large λ-expansions we shall obtain are valid in a sector greater than the right-half λ-plane, the expansion of $F_3(\lambda;z)$ for λ situated in the left-half plane can be obtained by application of the transformations (T1) and (T3) given in [2]. For such values of $\arg\lambda$, we may write $\lambda=\lambda' e^{\mp\pi i}$, with $|\arg\lambda'|<\frac{1}{2}\pi$, to find

$$F_3(\lambda;z)=(1-z)^{c-a-b+(\varepsilon_1+\varepsilon_2-1)\lambda'}\left\{Az^{1-c+\lambda'}\mathscr{F}_1+Bz^{b-c+(1-\varepsilon_2)\lambda'}\mathscr{F}_2\right\}, \tag{1.3}$$

where

$$\mathscr{F}_1\equiv F\left(\begin{matrix}1-a+\varepsilon_1\lambda', 1-b+\varepsilon_2\lambda'\\ 2-c+\lambda'\end{matrix};z\right),$$

$$\begin{aligned}\mathscr{F}_2&\equiv F\left(\begin{matrix}1-b+\varepsilon_2\lambda', c-b-(1-\varepsilon_2)\lambda'\\ 1+a-b+(\varepsilon_2-\varepsilon_1)\lambda'\end{matrix};\frac{1}{z}\right)\\ &=\left(1-\frac{1}{z}\right)^{b-1-\varepsilon_2\lambda'}F\left(\begin{matrix}1-b+\varepsilon_2\lambda', 1+a-c+(1-\varepsilon_1)\lambda'\\ 1+a-b+(\varepsilon_2-\varepsilon_1)\lambda'\end{matrix};\frac{1}{1-z}\right)\end{aligned} \tag{1.4}$$

and

$$A=\frac{e^{\pi i(c-\lambda')}\Gamma(c-1-\lambda')\Gamma(1+a-c+(1-\varepsilon_1)\lambda')\Gamma(1-b+\varepsilon_2\lambda')}{\Gamma(a-\varepsilon_1\lambda')\Gamma(c-b-(1-\varepsilon_2)\lambda')\Gamma(1-c+\lambda')},$$

$$B=\frac{e^{\pi i(c-b-(1-\varepsilon_2)\lambda')}\Gamma(1-b+\varepsilon_2\lambda')\Gamma(1+a-c+(1-\varepsilon_1)\lambda')}{\Gamma(1-c+\lambda')\Gamma(1+a-b+(\varepsilon_2-\varepsilon_1)\lambda')}.$$

Then, with $\varepsilon_1<\varepsilon_2$ and the rescaling $\lambda'\to(\varepsilon_2-\varepsilon_1)\lambda'$ in $\mathscr{F}_2$, it is seen that when $\varepsilon_2>1$ both functions $\mathscr{F}_1$ and $\mathscr{F}_2$ in (1.3) are of the same form as $F_3(\lambda;z)$ in (1.2) with $|\arg\lambda|<\frac{1}{2}\pi$. When $\varepsilon_1<\varepsilon_2<1$, the second representation of $\mathscr{F}_2$ in (1.4) is also of this form. In the case $\varepsilon_1=\varepsilon_2$, the function $\mathscr{F}_2$ can be seen to reduce to a function of Type B discussed in [2, §4].

As in [2], we shall employ the method of steepest descents applied to suitable integral representations of the function in (1.2). The resulting expansions are of Poincaré type and so break down in the neighbourhood of certain critical points in the z-plane. The asymptotic treatment in the neighbourhood of these points, or at a value of z corresponding to a Stokes phenomenon, is beyond the scope of the present paper and will be addressed elsewhere. We give numerical examples to illustrate the validity of the expansions so obtained.

2. The expansion of $F_3(\lambda;z)$ when $0<\varepsilon_1<1$

We first deal with the case $0<\varepsilon_1<1$ where it is supposed that $\varepsilon_1\leqslant\varepsilon_2$. From [2, (1.4)] we have the integral representation

$$F_3(\lambda;z)=\frac{\Gamma(c+\lambda)}{\Gamma(a+\varepsilon_1\lambda)\Gamma(c-a+(1-\varepsilon_1)\lambda)}\int_0^1 f(t)\,e^{\lambda\psi(t)}dt, \tag{2.1}$$

where the phase function $\psi(t)$ and amplitude function $f(t)$ are

$$\psi(t)=\varepsilon_1\log t+(1-\varepsilon_1)\log(1-t)-\varepsilon_2\log(1-zt),\qquad f(t)=\frac{t^{a-1}(1-t)^{c-a-1}}{(1-zt)^b}.$$

The t-plane is cut along $(-\infty,0]$ and $[1,\infty)$, and along the ray from the singularity at $1/z$ to infinity. The conditions in [2, (1.4)] on the integral in (2.1) are satisfied when $0<\varepsilon_1<1$ and λ is a complex variable which is initially taken to satisfy $|\arg\lambda|<\frac{1}{2}\pi$.

The phase function has saddle points where $\psi'(t)=0$; that is, at the points

$$t_{sj}=\frac{\Upsilon_{\mp}}{2(1-\varepsilon_2)z}=\frac{2\varepsilon_1}{\Upsilon_{\pm}}\qquad(j=1,2),\tag{2.2}$$

where the upper and lower signs correspond to $j=1$ and $j=2$ respectively and[1]

$$\Upsilon_{\pm}\equiv\Upsilon_{\pm}(z):=\Delta\pm\sqrt{\Delta^2-4\varepsilon_1(1-\varepsilon_2)z},\qquad\Delta:=1+(\varepsilon_1-\varepsilon_2)z.$$

The contribution to the integral in (2.1) (without the pre-factor) from the steepest descent path through the saddle point t_{sj} is given by the formal asymptotic sum

$$if(t_{sj})\,e^{\lambda\psi(t_{sj})+\pi i\gamma_j}\sqrt{\frac{2\pi}{\psi''(t_{sj})}}\sum_{k=0}^{\infty}\frac{c_k^{(j)}\Gamma(k+\frac{1}{2})}{\lambda^{k+\frac{1}{2}}\Gamma(\frac{1}{2})}\qquad(j=1,2)$$

as $|\lambda|\to\infty$, where

$$-\psi''(t_{sj})=\frac{\varepsilon_1(\varepsilon_2-\varepsilon_1)+t_{sj}(2\varepsilon_1-t_{sj})(1-\varepsilon_2)}{\varepsilon_2 t_{sj}^2(1-t_{sj})^2}\tag{2.3}$$

and the coefficients $c_k^{(j)}$ for $k\leqslant 2$ are given by [2, (2.4), (2.5)]. The γ_j are orientation factors that depend on the direction of integration $\arg(t-t_{sj})$ through the saddle point t_{sj} and have the value either 0 or 1. These factors are determined by

$$\arg(t-t_{sj})=-\tfrac{1}{2}\arg\lambda-\tfrac{1}{2}\arg\psi''(t_{sj})+\begin{cases}\frac{1}{2}\pi\\-\frac{1}{2}\pi\end{cases},\quad\gamma_j=\begin{cases}0\\1\end{cases},\tag{2.4}$$

where the branch of $\arg\psi''(t_{sj})$ is chosen throughout to be $[0,2\pi)$.

The above expansion will hold provided z is such that the saddle t_{sj} is not in a neighbourhood of a double saddle. The saddles t_{s1} and t_{s2} coalesce to form a double saddle (a turning point) when $\Delta^2-4\varepsilon_1(1-\varepsilon_2)z=0$; that is, when $z=z_*^{\pm}$, where

$$z_*^{\pm}=\frac{\varepsilon_1+\varepsilon_2-2\varepsilon_1\varepsilon_2\pm2\sqrt{\varepsilon_1\varepsilon_2(1-\varepsilon_1)(1-\varepsilon_2)}}{(\varepsilon_1-\varepsilon_2)^2}.\tag{2.5}$$

In the particular case $\varepsilon_1=\varepsilon_2\ (=\varepsilon)$, there is only a single (finite) value of z that results in the formation of a double saddle, which is given by the limit of $z_*^{\mp}$ as $\varepsilon_1\to\varepsilon_2$ according as $\varepsilon<1$ or $\varepsilon>1$, respectively; viz.

$$z_*=\frac{1}{4\varepsilon(1-\varepsilon)}=\lim_{\varepsilon_1\to\varepsilon_2}z_*^{\mp}\qquad\begin{cases}0<\varepsilon<1\\\varepsilon>1.\end{cases}\tag{2.6}$$

When $\varepsilon_1\leqslant\varepsilon_2<1$, it is not difficult to establish that the turning point (when $z=z_*^{\pm}$) lies on the interval $t\in[1,\infty)$, whereas when $\varepsilon_1<1$ and $\varepsilon_2>1$ it moves into the complex t-plane. When $\varepsilon_2\geqslant\varepsilon_1>1$, the turning point is situated on the negative real t-axis.

[1] It follows that $t_{s1}\,t_{s2}=\varepsilon_1\,z^{-1}/(1-\varepsilon_2)$.

2.1. The case $\varepsilon_1 \leqslant \varepsilon_2 < 1$

In the case of real z $(=x)$ satisfying $x<1$, it can be shown (we omit these details) that the saddles are situated on the real t-axis with $0<t_{s1}<1$ and $t_A<t_{s2}<\infty$ (when $0<x<1$) and $-\infty<t_{s2}<-t_B$ (when $x<0$), where

$$t_A=\begin{cases} 1 & \varepsilon_1+\varepsilon_2\leqslant 1 \\ \dfrac{\varepsilon_1}{|1-\varepsilon_2|} & \varepsilon_1+\varepsilon_2>1 \end{cases}, \qquad t_B=\frac{\varepsilon_2-\varepsilon_1}{|1-\varepsilon_2|}. \tag{2.7}$$

In this case the integration path in (2.1) is the path of steepest descent through the saddle t_{s1}. When z moves into the upper (resp. lower) half-plane it is found that t_{s1} and t_{s2} move into the upper (resp. lower) and lower (resp. upper) half-planes. The points $t=0$ and $t=1$ are zeros of the integrand for large $|\lambda|$ in $|\arg\lambda|<\frac{1}{2}\pi$, so that paths of steepest descent can terminate only at these points when $\varepsilon_2<1$, with paths of steepest ascent terminating at $t=1/z$ and infinity. Typical steepest descent paths through the saddles when z is complex are illustrated[2] in Fig. 1.

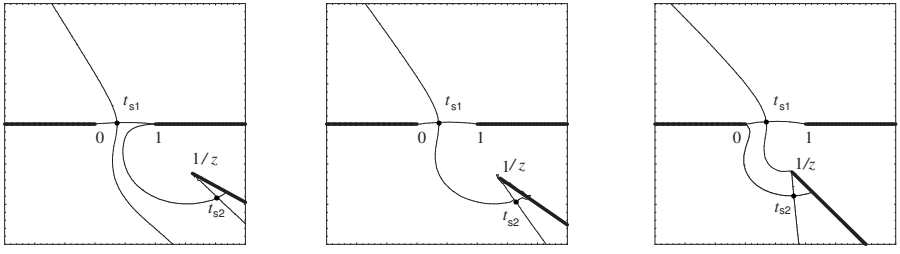

Figure 1: *Paths of steepest descent and ascent through the saddles t_{s1} and t_{s2} when* $\arg\lambda=0$ *and* $\varepsilon_1=\varepsilon_2=\frac{1}{3}$ *: (a) $z=0.40+0.30i$, (b) $z=0.40+0.37644i$ and (c) $z=0.40+0.60i$. The heavy lines denote branch cuts.*

The integration path $[0,1]$ can be reconciled with the path of steepest descent through t_{s1} to yield (with $\gamma_1=0$)

$$\begin{aligned} F_3(\lambda;z) &\sim \frac{2\pi i\Gamma(c+\lambda)}{\Gamma(a+\varepsilon_1\lambda)\Gamma(c-a+(1-\varepsilon_1)\lambda)}\,\frac{f(t_{s1})e^{\lambda\psi(t_{s1})}}{\sqrt{2\pi\psi''(t_{s1})}}\sum_{k=0}^{\infty}\frac{c_k^{(1)}\Gamma(k+\frac{1}{2})}{\lambda^{k+\frac{1}{2}}\Gamma(\frac{1}{2})} \\ &= \frac{2\pi i\Gamma(c+\lambda)}{\Gamma(a+\varepsilon_1\lambda)\Gamma(c-a+(1-\varepsilon_1)\lambda)} \\ &\quad\times\frac{t_{s1}^{a-1+\varepsilon_1\lambda}(1-t_{s1})^{-\nu}}{\sqrt{2\pi\psi''(t_{s1})}\,(1-zt_{s1})^{b+\varepsilon_2\lambda}}\sum_{k=0}^{\infty}\frac{c_k^{(1)}\Gamma(k+\frac{1}{2})}{\lambda^{k+\frac{1}{2}}\Gamma(\frac{1}{2})}, \qquad (0<\varepsilon_1\leqslant\varepsilon_2<1) \end{aligned} \tag{2.8}$$

[2]We remark that although Fig. 1(b) illustrates a connection between the saddles, this does not result in a Stokes phenomenon for the integral in (2.1) since the integration path runs from $t=0$ to $t=1$.

as $|\lambda| \to \infty$ in the sector $|\arg\lambda| < \frac{1}{2}\pi$, where for convenience we have set

$$\nu \equiv \nu(\lambda) := a - c + 1 + (\varepsilon_1 - 1)\lambda. \tag{2.9}$$

This expansion will cease to be valid in a neighbourhood of a double saddle; that is, when z is close to the values $z_*^{\pm}$, or the value z_* if $\varepsilon_1 = \varepsilon_2$.

The sector of validity of the expansion (2.8) can be extended by means of the arguments described in [2, §2.2]. From [2, (3.11)], the sector of validity can be extended to $|\arg\lambda| \leqslant \pi - \delta$ for values of z situated in the domain in which $\xi > 0$, where

$$\psi(t_{s1}) - \psi(t_{s2}) \equiv \xi + i\eta \tag{2.10}$$

and ξ, η are real. Some routine algebra making use of (2.2) shows that $\xi = 0$ when

$$\left| \frac{\Upsilon_-}{\Upsilon_+} \left(\frac{\Upsilon_+ - 2\varepsilon_1}{\Upsilon_- - 2\varepsilon_1} \right)^{1-\varepsilon_1} \left(\frac{\Upsilon_+ - 2(1-\varepsilon_2)}{\Upsilon_- - 2(1-\varepsilon_2)} \right)^{\varepsilon_2} \right| = 1. \tag{2.11}$$

Examples of the curves in the z-plane in the vicinity of the interval $[0,1]$ on which $\xi = 0$ are shown in Fig. 2; the node on the real axis to the right of $z = 1$ corresponds to the point $z = z_*^-$. Also displayed is the curve (shown dashed) on which $\eta = 0$, where the saddles become connected; see Fig. 1(b). However, in the case of the integral in (2.1) taken between the endpoints $t = 0$ and $t = 1$, this does *not* result in a Stokes phenomenon. In the domain surrounding the point $z = 1$ (shown shaded) the quantity $\xi > 0$; in this domain the sector of validity of (2.8) is given by

$$-\tfrac{1}{2}\pi - \omega_- + \delta < \arg\lambda < \tfrac{1}{2}\pi + \omega_+ - \delta, \tag{2.12}$$

where

$$\omega_\pm = \arctan\left(\frac{2\pi \mp \eta}{\xi} \right), \qquad \omega_\mp = \pm \arctan(\eta/\xi), \tag{2.13}$$

with the upper or lower signs corresponding to $\eta > 0$ and $\eta < 0$, respectively. Outside of this domain, $\xi < 0$ and $\omega_\pm = \frac{1}{2}\pi$, so that the expansion (2.8) holds in the wider sector $|\arg\lambda| \leqslant \pi - \delta$.

2.2. The case $\varepsilon_1 = \varepsilon_2 < 1$

In the special case $\varepsilon_1 = \varepsilon_2 = \varepsilon < 1$, the expression (2.11) reduces to

$$\left| \frac{\Upsilon_-}{\Upsilon_+} \left(\frac{\Upsilon_+ - 2\varepsilon}{\Upsilon_- - 2\varepsilon} \right)^{1-2\varepsilon} \right| = 1. \tag{2.14}$$

An example of this curve is shown in Fig. 2(b) where the vertex on the right of $z = 1$ is the value z_*. When $\varepsilon = \frac{1}{3}$, the domain bounded by (2.14) agrees with that obtained in [3, p. 305] with $z_* = \frac{9}{8}$. In this case a little algebra shows that the leading term of (2.8) agrees with the asymptotic behaviour given in [3, p. 207].

The case $\varepsilon = \frac{1}{2}$ (corresponding to Riemann's example – see [2, §1]) is worthy of special mention. It is not difficult to see from (2.14) that in this case the curves on which

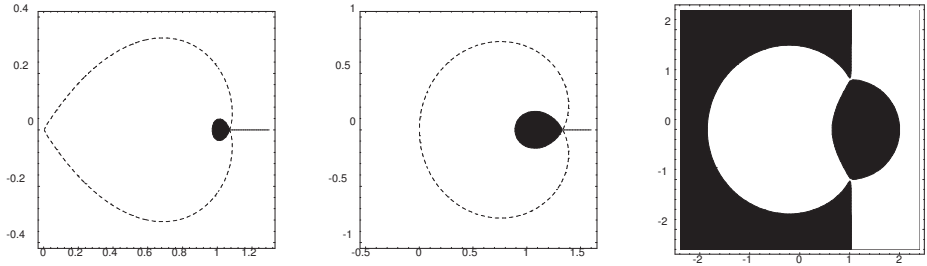

Figure 2: *The domain in the z-plane in which $\xi > 0$ (shaded) and the curve $\eta = 0$ (dashed) when (a) $\varepsilon_1 = 0.25$, $\varepsilon_2 = 0.50$, (b) $\varepsilon_1 = \varepsilon_2 = 0.25$ and (c) $\varepsilon_1 = 0.50$, $\varepsilon_2 = 1.20$; outside the shaded domains $\xi < 0$ except on the line issuing from the node where $\xi = 0$. In (c) the vertices of the crescent-shaped domain where $\xi < 0$ correspond to $z_*^{\pm}$ and the vertical lines from these points are branch cuts.*

$\xi = 0$ are symmetrical about $\varepsilon = \frac{1}{2}$; that is, the curves corresponding to $\varepsilon = \frac{1}{2} \pm \varepsilon'$ ($0 < \varepsilon' < \frac{1}{2}$) are the same. In addition, the domain about the point $z = 1$ where $\xi > 0$ shrinks to zero as $\varepsilon \to \frac{1}{2}$. This follows from the fact that when $\varepsilon = \frac{1}{2}$ (2.14) reduces to

$$\left| \frac{1 - \sqrt{1-z}}{1 + \sqrt{1-z}} \right| = 1.$$

With $1 - z = \rho e^{i\varphi}$, this yields $\rho^{1/2} \cos \frac{1}{2}\varphi = 0$, whence $\rho = 0$ or $\varphi = \pm\pi$. Consequently, when $\varepsilon = \frac{1}{2}$, the curve on which $\xi = 0$ consists only of the interval $[1, \infty)$ in the z-plane.

Finally, as $\varepsilon \to 1^-$, we see that $z_*^- \to +\infty$ and (2.14) becomes in the limit

$$\left| \frac{z}{z-1} \right| = 1 \quad \text{or} \quad \mathrm{Re}\,(z) = \tfrac{1}{2}.$$

Thus, as $\varepsilon \to 1^-$, the expansion (2.8) holds in the wider sector $|\arg \lambda| \leqslant \pi - \delta$ when $\mathrm{Re}\,(z) \leqslant \frac{1}{2}$, which agrees with the domain of validity of the standard result quoted in [2, (1.2)] combined with the transformation (T1).

2.3. The case $\varepsilon_1 < 1$, $\varepsilon_2 > 1$

When $\varepsilon_1 < 1$, $\varepsilon_2 > 1$ and z is real, the saddle t_{s1} again satisfies $0 < t_{s1} < 1$ for $x < 1$, with the saddle t_{s2} situated in the intervals $-\infty < t_{s2} < -t_A$ (when $0 < x < 1$) and $t_B < t_{s2} < \infty$ (when $x < 0$), where t_A and t_B are defined in (2.7). When z is in the upper (resp. lower) half-plane, both saddles are situated in the upper (resp. lower) half-plane and further interaction between them now becomes possible. When $\varepsilon_2 > 1$, we observe that paths of steepest descent can also terminate at infinity, in addition to the points $t = 0$ and $t = 1$, since the exponential factor in the integrand is $\mathrm{O}(\exp[t^{\lambda(1-\varepsilon_2)}])$ as $t \to \infty$.

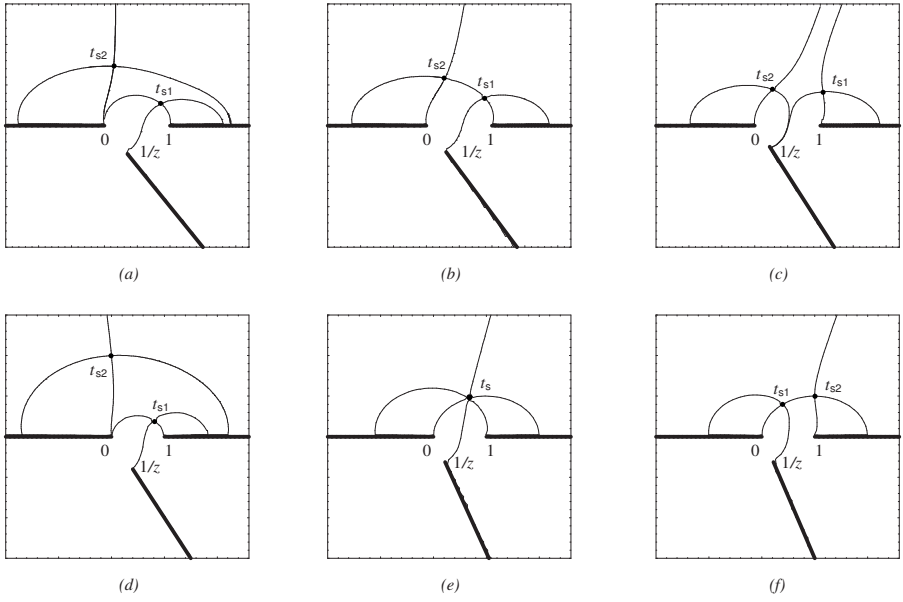

Figure 3: *Paths of steepest descent and ascent through the saddles t_{s1} and t_{s2} when* $\arg\lambda = 0$ *and* $\varepsilon_1 = \frac{2}{3}$, $\varepsilon_2 = \frac{4}{3}$ *: (a)* $z = 0.60 + 1.20i$, *(b)* $z = 0.60 + 1.35036i$, *(c)* $z = 0.60 + 1.50i$, *(d)* $z = 0.50 + i$, *(e)* $z = 0.50 + i\sqrt{2}$ *and (f)* $z = 0.50 + 1.50i$. *The heavy lines denote branch cuts.*

Typical steepest descent paths are shown in Fig. 3 for the case $\varepsilon_1 = \frac{2}{3}$, $\varepsilon_2 = \frac{4}{3}$, $\lambda > 0$ and a sequence of z values. We note from (2.5) that $z_*^{\pm} = \frac{1}{2} \pm i\sqrt{2}$ for these values of ε_1 and ε_2. In Fig. 3(a)–(c) we show the paths when $z = 0.60 + iy$, with three different values of $y > 0$. When $y = 1.20$ only the saddle t_{s1} contributes to the integral (2.1); when $y \doteq 1.35036$ the saddles connect to produce a Stokes phenomenon; and when $y = 1.5$ both saddles contribute. The integration path in this last case emanates from $t = 0$, passing to infinity over the saddle t_{s2}, and returns from infinity over the saddle t_{s1} to terminate at $t = 1$. In Fig. 3(d)–(f) we show the paths when $z = 0.50 + iy$ for three different values of $y > 0$; when $y = \sqrt{2}$, so that $z = z_*^+ = \frac{1}{2} + i\sqrt{2}$, the saddles coalesce to form a double saddle.

An example of the curves in the z-plane where $\xi = 0$ is repeated in Fig. 4(a) where, in addition, the Stokes curves on which $\eta = 0$ (when $\arg\lambda = 0$) that result in a Stokes phenomenon are shown dashed. It should be noted that a third Stokes curve emanating from z_*^+ and terminating at $z = 0$ has not been shown as no Stokes phenomenon associated with the integral in (2.1) is found to take place on this latter curve; a similar remark applies to z_*^-. The vertices of the crescent-shaped domain (where $\xi < 0$) correspond to the points $z_*^{\pm}$. In Fig. 4(b) we show the locus of $z = z_*^+$ in the upper half of the z-plane[3] as a function of ε_2 when $\varepsilon_1 = 0.50$ corresponding to the formation of a double saddle in the t-plane. The behaviour of z_*^- in the lower half-plane

[3]From (2.5) it is easily seen that $z_*^{\pm} \to (1 - \varepsilon_1)^{-1}$ as $\varepsilon_2 \to 1^+$ and $z_*^{\pm} \to 0$ for large ε_2.

is the conjugate image. Also shown in the figure are the two Stokes curves issuing from z_*^+ for different values of ε_2 (when $\lambda > 0$) that result in a Stokes phenomenon. As one crosses a particular curve from left to right the saddle t_{s2} switches on. We remark that it is possible for more than one Stokes phenomenon to occur as Im (z) varies at fixed Re (z). For example, when $\varepsilon_2 = 1.3$ and $z = 1 + iy$ a Stokes phenomenon occurs for $y \doteq 0.61853$ and $y \doteq 1.61673$.

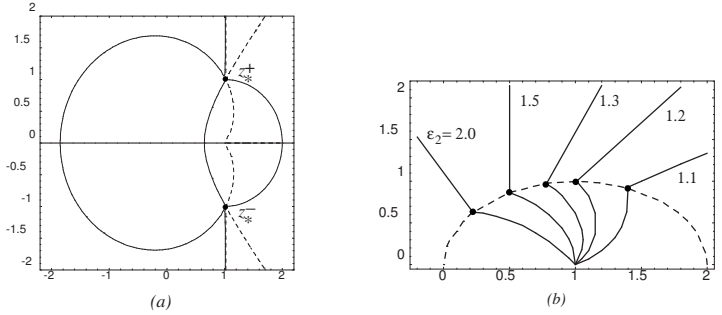

Figure 4: *(a) The curves in the z-plane on which $\xi = 0$ (solid) and $\eta = 0$ (dashed) when $\varepsilon_1 = 0.50$ and $\varepsilon_2 = 1.20$. The heavy dots denote the points $z_*^{\pm}$. (b) The locus (dashed curve) of z_*^+ in the upper-half z-plane corresponding to the formation of a double saddle point when* $\arg\lambda = 0$ *and $\varepsilon_1 = 0.50$ as a function of $\varepsilon_2 > 1$. The solid curves show the values of z for different ε_2 for which $\eta = 0$ (the Stokes curves) to produce a Stokes phenomenon; the heavy dots denote the corresponding values of z_*^+. The curves in the lower half-plane are the conjugate images.*

In regions of the z-plane where only the saddle t_{s1} contributes the expansion of $F_3(\lambda;z)$ is given by (2.8). When both saddles contribute we have the expansion

$$F_3(\lambda;z) \sim \frac{2\pi i\Gamma(c+\lambda)}{\Gamma(a+\varepsilon_1\lambda)\Gamma(c-a+(1-\varepsilon_1)\lambda)} \left\{ \frac{f(t_{s1})\, e^{\lambda\psi(t_{s1})+\pi i\gamma_1}}{\sqrt{2\pi\psi''(t_{s1})}} \sum_{k=0}^{\infty} \frac{c_k^{(1)}\Gamma(k+\frac{1}{2})}{\lambda^{k+\frac{1}{2}}\Gamma(\frac{1}{2})} \right.$$
$$\left. + \frac{f(t_{s2})\, e^{\lambda\psi(t_{s2})+\pi i\gamma_2}}{\sqrt{2\pi\psi''(t_{s2})}} \sum_{k=0}^{\infty} \frac{c_k^{(2)}\Gamma(k+\frac{1}{2})}{\lambda^{k+\frac{1}{2}}\Gamma(\frac{1}{2})} \right\} \tag{2.15}$$

for $|\lambda| \to \infty$, where the orientation factors γ_1 and γ_2 are determined from (2.8). The λ-domain of validity of this composite expansion is discussed in [2, §4.3]; see (4.14) therein. The expansion for complex λ in the left-hand plane can be obtained from (1.3).

2.4. Numerical results

In this section we present the results of numerical calculations of the hypergeometric function $F_3(\lambda;z)$ defined in (2.1) with $\varepsilon_1 < 1$, $\varepsilon_1 \leqslant \varepsilon_2$ and its asymptotic representation in (2.8). For real λ and real values of z $(= x)$ in the range $x < 1$, we show in Table 1 the values of $F_3(\lambda;x)$ and the absolute relative error using the truncation index $k = 2$ in the asymptotic expansion.

Table 1: Values of $F_3(\lambda;x)$ and the absolute relative error resulting from the asymptotic expansion (2.8) (with $k \leqslant 2$) when $x < 1$. The values shown correspond to $\lambda = 40$ with $a = \frac{1}{4}$, $b = \frac{1}{2}$, $c = \frac{3}{4}$ and three sets of values of ε_1, ε_2.

	$\varepsilon_1 = 0.25,\ \varepsilon_2 = 0.40$		$\varepsilon_1 = \varepsilon_2 = 0.25$		$\varepsilon_1 = 0.50,\ \varepsilon_2 = 1.20$	
x	$F_3(\lambda;x)$	Rel. Error	$F_3(\lambda;x)$	Rel. Error	$F_3(\lambda;x)$	Rel. Error
0.75	6.30919(+1)	2.376(−6)	1.17533(+1)	1.334(−6)	2.27456(+15)	1.338(−6)
0.50	1.16561(+1)	7.490(−7)	4.51425(+1)	9.495(−7)	3.04454(+7)	4.219(−7)
0.25	3.06503(+0)	5.533(−7)	2.01760(+0)	6.277(−7)	1.12575(+3)	7.757(−7)
−0.50	1.60013(−1)	3.426(−7)	3.03632(−1)	4.411(−7)	6.84559(−5)	9.151(−7)
−1.00	3.63117(−2)	1.171(−7)	1.11898(−1)	1.134(−7)	9.38275(−8)	1.101(−6)

Table 2: Values of the absolute relative error in $F_3(\lambda;z)$ resulting from the asymptotic expansions (2.8) and (2.15) (with $k \leqslant 2$) when $\lambda = 80e^{i\theta}$ for different θ and $a = \frac{1}{4}$, $b = \frac{1}{2}$, $c = \frac{3}{4}$.

	$\varepsilon_1 = \varepsilon_2 = 0.25$ $z = 0.50\ \ (\xi < 0)$			$\varepsilon_1 = 0.25,\ \varepsilon_2 = 0.40$ $z = 0.50 + 0.50i\ \ (\xi < 0)$		
θ/π	Rel. Error	θ/π	Rel. Error	θ/π	Rel. Error	θ/π	Rel. Error
0	1.117(−7)			0	7.512(−8)		
0.20	1.104(−7)	−0.20	1.104(−7)	0.20	8.165(−8)	−0.20	6.931(−8)
0.40	1.070(−7)	−0.40	1.070(−7)	0.40	8.668(−8)	−0.40	6.801(−8)
0.60	1.027(−7)	−0.60	1.027(−7)	0.60	8.871(−8)	−0.60	6.911(−8)
0.80	9.901(−8)	−0.80	9.901(−8)	0.80	8.704(−8)	−0.80	7.514(−8)
0.90	9.795(−8)	−0.90	9.795(−8)	0.90	8.488(−8)	−0.90	7.866(−8)
0.95	1.003(−7)	−0.95	1.003(−7)	0.95	8.438(−8)	−0.95	7.849(−8)
	$\varepsilon_1 = 0.50,\ \varepsilon_2 = 1.20$ $z = -1 + i\ \ (\xi < 0)$			$\varepsilon_1 = 0.50,\ \varepsilon_2 = 1.20$ $z = 1.50 + 0.50i\ \ (\xi > 0)$		
θ/π	Rel. Error	θ/π	Rel. Error	θ/π	Rel. Error	θ/π	Rel. Error
0	2.899(−7)			0	2.688(−5)		
0.20	2.835(−7)	−0.20	2.965(−7)	0.20	3.172(−5)	−0.20	2.880(−5)
0.40	2.792(−7)	−0.40	3.005(−7)	0.50	2.595(−5)	−0.50	2.817(−5)
0.60	2.784(−7)	−0.60	2.999(−7)	0.80	2.626(−5)	−0.60	2.728(−5)
0.80	2.814(−7)	−0.80	2.948(−7)	0.90	2.547(−5)	−0.65	2.035(−5)
0.90	2.842(−7)	−0.90	2.913(−7)	0.95	2.513(−5)	−0.75	6.174(−3)
0.95	2.858(−7)	−0.95	2.894(−7)	0.99	3.622(−4)	−0.80	2.329(−1)

Table 2 shows values of the error in the computation of $F_3(\lambda;x)$ using (2.8) and (2.15) for complex values of λ and different values of z. The first three values of z selected correspond to the domain in the z-plane where $\xi < 0$, so that the expansion (2.8) in these cases is valid in the wider sector $|\arg\lambda| \leqslant \pi - \delta$. The final entry is for $z = 1.50 + 0.50i$ with $\varepsilon_1 = 0.50$ and $\varepsilon_2 = 1.20$, which is situated to the right of the $\eta = 0$ curve in Fig. 4(a) so that (2.15) is applicable. These values correspond to $(\xi,\eta) = (0.156, 0.247)$, so that the expansion (2.15) is valid for $|\lambda| \to \infty$ in the reduced sector (2.12), where $\omega_+ = 0.492\pi$ and $\omega_- = 0.321\pi$ from (2.13).

3. The expansion of $F_3(\lambda;z)$ when $\varepsilon_2 \geqslant \varepsilon_1 > 1$

When $\varepsilon_2 \geqslant \varepsilon_1 > 1$, we employ the integral representation for $F_3(\lambda;z)$ given in [2, (1.5)]

$$F_3(\lambda;z) = \frac{\Gamma(c+\lambda)\Gamma(1-c+a+(\varepsilon_1-1)\lambda)}{2\pi i\Gamma(a+\varepsilon_1\lambda)} \int_0^{(1+)} f(t)\, e^{\lambda\psi(t)} dt \tag{3.1}$$

valid for $|\arg\lambda| < \frac{1}{2}\pi$ and $|\arg(1-z)| < \pi$, where the phase function $\psi(t)$ and amplitude function $f(t)$ are

$$\psi(t) = \varepsilon_1 \log t + (1-\varepsilon_1)\log(t-1) - \varepsilon_2 \log(1-zt), \qquad f(t) = \frac{t^{a-1}(t-1)^{c-a-1}}{(1-zt)^b}. \tag{3.2}$$

The integration path is a loop surrounding the point $t = 1$ in the positive sense that starts and terminates at $t = 0$, but excludes the branch point $t = 1/z$. The t-plane is cut along $[-\infty, 1]$ and along the ray from $1/z$ to infinity in a suitable direction. The phase function has saddle points at t_{s1} and t_{s2} given by (2.2)

3.1. Real z

We consider first the case of real z $(= x)$ satisfying $x < 1$. When $\varepsilon_2 > \varepsilon_1 > 1$, the quantities $z_*^{\pm}$ defined in (2.5) are real and satisfy $z_*^- < z_*^+ < 0$. There are four ranges of x to consider, namely (i) $0 < x < 1$, (ii) $z_*^+ \leqslant x < 0$, (iii) $z_*^- < x < z_*^+$ and (iv) $x \leqslant z_*^-$. When $\varepsilon_1 = \varepsilon_2 = \varepsilon > 1$, there is only one value of z that results in a double saddle given by $z_* = -1/\{4\varepsilon(\varepsilon-1)\}$ from (2.6). In this case there are three ranges of x to consider, namely (i) $0 < x < 1$, (ii) $z_* \leqslant x < 0$ and (iii) $x < z_*$.

When $0 < x < 1$ and $\varepsilon_2 \geqslant \varepsilon_1 > 1$, the saddles are situated on the real t-axis with $1 < t_{s1} < 1/x$ and $-\infty < t_{s2} < -t_A$, where t_A is defined in (2.7). When $z_*^+ \leqslant x < 0$, the saddle t_{s1} progressively moves to the right as x decreases, with t_{s2} now situated on the positive real axis such that $t_{s1} \leqslant t_{s2} < \infty$; when $x = z_*^+$ the saddles coalesce to form a double saddle. When $z_*^- < x < z_*^+$ $(\varepsilon_2 > \varepsilon_1)$, the saddles move off the real axis to become a conjugate pair; $|\mathrm{Im}\,(t_{sj})|$ at first increases and then decreases to zero as $x \to z_*^-$, with $\mathrm{Re}\,(t_{sj})$ steadily decreasing as x decreases in this interval. A similar behaviour occurs when $\varepsilon_1 = \varepsilon_2$ for $x < z_*$, except that $t_{s1}, t_{s2} \to 0$ as $x \to -\infty$. Finally, when $x \leqslant z_*^-$ $(\varepsilon_2 > \varepsilon_1)$ the saddles are situated on the real t-axis again forming a double saddle when $x = z_*^-$, with $t_{s1} \to 0$ and $t_{s2} \to t_B < 1$ as $x \to -\infty$.

In Fig. 5 we show typical paths of steepest descent for the cases $z_*^+ < x < 1$, $z_*^- < x < z_*^+$ and $x < z_*^-$ when $\varepsilon_2 > \varepsilon_1 > 1$. When $z_*^+ < x < 1$, the path of steepest descent through t_{s1} is a loop emanating from the origin that surrounds the point $t = 1$; see Fig. 5(a). The expansion is then (with $\gamma_1 = 0$ and $\psi''(t_{s1}) > 0$)

$$F_3(\lambda;x) \sim \frac{\Gamma(c+\lambda)\Gamma(1-c+a+(\varepsilon_1-1)\lambda)}{\Gamma(a+\varepsilon_1\lambda)} \frac{f(t_{s1})e^{\lambda\psi(t_{s1})+\pi i\gamma_1}}{\sqrt{2\pi\psi''(t_{s1})}} \sum_{k=0}^{\infty} \frac{c_k^{(1)}\Gamma(k+\frac{1}{2})}{\lambda^{k+\frac{1}{2}}\Gamma(\frac{1}{2})}$$

$$(z_*^+ < x < 1,\ \varepsilon_2 \geqslant \varepsilon_1 > 1). \tag{3.3}$$

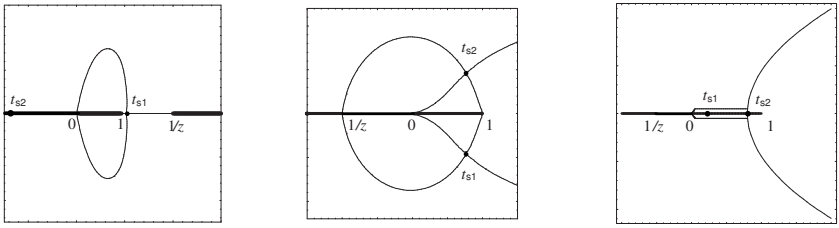

Figure 5: *Paths of steepest descent and ascent through the saddles* t_{s1} *and* t_{s2} *when* $\arg\lambda = 0$ *and* $\varepsilon_1 = 1.20$, $\varepsilon_2 = 2.50$*: (a)* $z = 0.50$*, (b)* $z = -1.00$ *and (c)* $z = -2.80$*. The heavy lines denote branch cuts. In (a) and (c) the steepest ascent paths through* t_{s2} *and* t_{s1} *(not shown) terminate at the point* $1/z$*.*

When $z_*^- < x < z_*^+$ $(\varepsilon_2 > \varepsilon_1)$, or $x < z_*$ $(\varepsilon_1 = \varepsilon_2)$, the integration path in (3.1) can be expanded to coincide with the steepest path through t_{s1} in the lower half-plane that passes to infinity and returns along the steepest path through t_{s2} in the upper half-plane; see Fig. 5(b). In this case the expansion is given by (with $\gamma_1 = 0$, $\gamma_2 = 1$)

$$F_3(\lambda;x) \sim \frac{\Gamma(c+\lambda)\Gamma(1-c+a+(\varepsilon_1-1)\lambda)}{\Gamma(a+\varepsilon_1\lambda)} \left\{ \frac{f(t_{s1})\,e^{\lambda\psi(t_{s1})+\pi i\gamma_1}}{\sqrt{2\pi\psi''(t_{s1})}} \sum_{k=0}^{\infty} \frac{c_k^{(1)}\Gamma(k+\frac{1}{2})}{\lambda^{k+\frac{1}{2}}\Gamma(\frac{1}{2})} \right.$$
$$\left. + \frac{f(t_{s2})\,e^{\lambda\psi(t_{s2})+\pi i\gamma_2}}{\sqrt{2\pi\psi''(t_{s2})}} \sum_{k=0}^{\infty} \frac{c_k^{(2)}\Gamma(k+\frac{1}{2})}{\lambda^{k+\frac{1}{2}}\Gamma(\frac{1}{2})} \right\}$$

$$(z_*^- < x < z_*^+,\ \varepsilon_2 > \varepsilon_1 > 1;\ x < z_*,\ \varepsilon_1 = \varepsilon_2 > 1). \tag{3.4}$$

Finally, when $x < z_*^-$ $(\varepsilon_2 > \varepsilon_1)$ the steepest path between $t = 0$ and t_{s2} coincides with the real axis on the lower side of the branch cut, passing over the dominant saddle t_{s1} where $\psi''(t_{s1}) < 0$. At t_{s2}, the steepest path turns through $-\frac{1}{2}\pi$ and passes to infinity. The steepest path in the upper half-plane is the symmetrical image of that in the lower half-plane and passes to the origin over the saddle t_{s1} on the upper side of the cut; see Fig. 5(c). Taking into account the behaviour of the factor $(t_{s1}-1)^{-\nu}$ on both sides of the cut, where ν is defined in (2.9), we obtain

$$F_3(\lambda;x) \sim \frac{2\sin(\pi\nu)\Gamma(c+\lambda)\Gamma(1-c+a+(\varepsilon_1-1)\lambda)}{\Gamma(a+\varepsilon_1\lambda)} \frac{\hat{f}(t_{s1})\,e^{\lambda\hat{\psi}(t_{s1})}}{\sqrt{2\pi|\psi''(t_{s1})|}} \sum_{k=0}^{\infty} \frac{c_k^{(1)}\Gamma(k+\frac{1}{2})}{\lambda^{k+\frac{1}{2}}\Gamma(\frac{1}{2})}$$

$$(x < z_*^-,\ \varepsilon_2 > \varepsilon_1 > 1;\ \nu \neq \mathbf{N}). \tag{3.5}$$

The quantities $\hat{f}(t)$ and $\hat{\psi}(t)$ are as defined in (3.2), but with $t-1$ replaced by $1-t$. When $\nu = \mathbf{N}$, where $\mathbf{N}$ is a positive integer, the sine factor in (3.5) vanishes. In this case the contribution taken between $t = 0$ and t_{s2} cancels and we are left with the contribution from the subdominant saddle t_{s2}: half the contribution leaving t_{s2} in the

lower half-plane and half entering t_{s2} in the upper half-plane. Thus we find (with $\gamma_2 = 1$ and $\psi''(t_{s2}) > 0$)

$$F_3(\lambda;x) \sim \frac{\Gamma(c+\lambda)\Gamma(1-c+a+(\varepsilon_1-1)\lambda)}{\Gamma(a+\varepsilon_1\lambda)} \frac{f(t_{s2})\,e^{\lambda\psi(t_{s2})+\pi i}}{\sqrt{2\pi\psi''(t_{s2})}} \sum_{k=0}^{\infty} \frac{c_k^{(2)}\Gamma(k+\frac{1}{2})}{\lambda^{k+\frac{1}{2}}\Gamma(\frac{1}{2})}$$

$$(x < z_*^-,\ \varepsilon_2 > \varepsilon_1 > 1,\ \nu = \mathbf{N}). \qquad (3.6)$$

In each of (3.3) – (3.6), the coefficients $c_k^{(j)}$ are obtained from [2, (3.4), (3.5)] and $\psi''(t_{sj})$ is given by (2.3). Again, it must be emphasised that the branch of $\arg\psi''(t_{sj})$ in (3.4) is chosen to be $[0, 2\pi)$; see the comment after (2.4).

3.2. Complex λ and z

When $\arg\lambda \neq 0$, the above steepest descent paths are modified principally by the introduction of a spiral approach to the singular points $t = 0$ and $t = 1/z$. When z is complex, the point $t = 1/z$ moves off the positive real axis into the complex plane to produce typical steepest paths as illustrated in Fig. 6 (when $\arg\lambda = 0$), where we show a sequence of z values with $\mathrm{Re}\,(z) = 0.50$. It is seen that the saddles t_{s1} and t_{s2} connect for a certain value of $\mathrm{Im}\,(z)$ to produce a Stokes phenomenon.

The Stokes curve in the z-plane on which $\eta = 0$ (see (2.10)) for the particular choice of the parameters $\varepsilon_1 = 1.20$ and $\varepsilon_2 = 2.50$ is shown by the dashed curve in Fig. 7. Inside this curve only the saddle t_{s1} contributes to the integral (3.1) with the expansion of $F_3(\lambda;z)$ given by (3.3); outside this curve, both saddles contribute and the expansion is given by (3.4), with the orientation factors γ_j in each case determined by (2.4). The shaded domain in Fig. 7 corresponds to the region in which $\xi < 0$, where the expansion (3.3) holds for $|\lambda| \to \infty$ in $|\arg\lambda| \leqslant \pi - \delta$; outside this domain, we have $\xi > 0$ (except on the line issuing from the node where $\xi = 0$) and the expansion (3.3) will hold in the reduced sector (2.12). The validity of the expansion (3.4) is determined from [2, (4.14)].

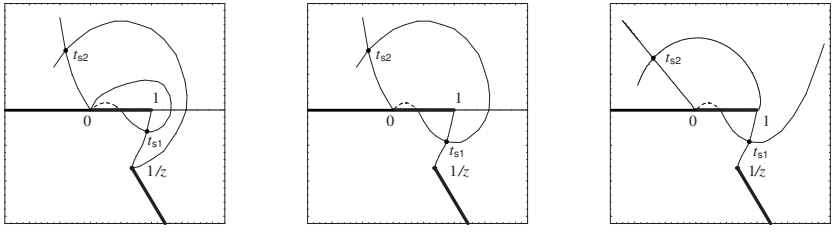

Figure 6: *Paths of steepest descent and ascent through the saddles t_{s1} and t_{s2} when* $\arg\lambda = 0$ *and* $\varepsilon_1 = 1.20$, $\varepsilon_2 = 2.50$*: (a) $z = 0.50 + 0.50i$, (b) $z = 0.50 + 0.52229i$ and (c) $z = 0.50 + i$. The heavy lines denote branch cuts.*

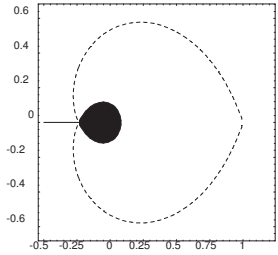

Figure 7: *The domain in the z-plane in which $\xi < 0$ (shaded) and the curve $\eta = 0$ (dashed) when $\varepsilon_1 = 1.20$ and $\varepsilon_2 = 2.50$. Outside the shaded domain $\xi > 0$ except on the line issuing from the node z_*^+ where $\xi = 0$.*

3.3. Numerical results

We present the results of numerical calculations of the hypergeometric function $F_3(\lambda;z)$ defined in (2.1) with $\varepsilon_2 \geqslant \varepsilon_1 > 1$ and its various asymptotic representations. For real λ and real values of z $(= x)$ in the three ranges $z_*^+ < x < 1$, $z_*^- < x < z_*^+$ and $x < z_*^-$, we show in Tables 3 and 4 the values of $F_3(\lambda;x)$ and the absolute relative error using the truncation index $k = 2$ in the asymptotic expansions. The particular case chosen corresponds to $\varepsilon_1 = 1.20$, $\varepsilon_2 = 2.50$, for which $z_*^+ \doteq -0.23825$ and $z_*^- \doteq -2.48365$. In Table 3, corresponding to the range $z_*^- < x < 1$, the asymptotic values are obtained from (3.3) and (3.4). The values shown in Table 4 correspond to the range $x < z_*^-$ and noninteger (upper figures) and integer values (lower figures) of $\nu := c - a + 1 + (\varepsilon_1 - 1)\lambda$. The asymptotic approximations employed are those in (3.5) and (3.6).

Table 3: Values of $F_3(\lambda;x)$ and the absolute relative error resulting from the asymptotic expansion (3.3) (with $k \leqslant 2$) when $z_*^- < x < 1$. The values shown correspond to $\lambda = 40$ and two sets of values of ε_1, ε_2 with $a = \frac{1}{4}$, $b = \frac{1}{2}$, $c = \frac{3}{4}$.

	$\varepsilon_1 = 1.20,\ \varepsilon_2 = 2.50$		$\varepsilon_1 = \varepsilon_2 = 1.50$	
x	$F_3(\lambda;x)$	Rel. Error	$F_3(\lambda;x)$	Rel. Error
0.75	+2.12737(+64)	4.645(−6)	+2.81974(+50)	3.154(−7)
0.50	+1.69875(+34)	4.666(−6)	+5.39572(+25)	3.589(−7)
0.25	+3.02852(+14)	4.868(−6)	+7.99433(+10)	4.882(−7)
−0.10	+9.99825(−06)	4.375(−5)	+1.78640(−04)	8.755(−6)
−1.00	−4.35190(−36)	2.701(−5)	−1.89498(−29)	2.349(−5)

Table 5 shows values of the absolute relative error in the computation of $F_3(\lambda;x)$ using (3.3) for three different values of x in the range $z_*^- < x < 1$ and complex values of λ. In the case $x = 0.50$, the quantities ξ and η defined in (2.10) have the values $\xi = 3.614$, $\eta = \pi$; from (2.13) this yields $\omega_\pm = 0.228\pi$. It then follows from (2.12) that the sector of validity of (3.3) for this value of x can be extended to $|\arg\lambda| \leqslant$

Table 4: Values of $F_3(\lambda;x)$ and the absolute relative error resulting from the asymptotic expansions (3.5) and (3.6) (with $k \leqslant 2$) when $x < z_*^-$. The values shown correspond to $\varepsilon_1 = 1.20$, $\varepsilon_2 = 2.50$ and $a = \frac{1}{4}$, $b = \frac{1}{2}$.

	$x=-4.00,\ \lambda=40$		$x=-5.00,\ \lambda=40$	
c	$F_3(\lambda;x)$	Rel. Error	$F_3(\lambda;x)$	Rel. Error
0.75	+6.85587(−68)	8.632(−4)	+7.92658(−73)	1.026(−4)
1.25	−1.02799(−71)	1.198(−3)	−2.29467(−79)	2.753(−4)
	$x=-4.00,\ \lambda=41$		$x=-5.00,\ \lambda=41$	
c	$F_3(\lambda;x)$	Rel. Error	$F_3(\lambda;x)$	Rel. Error
0.75	+1.14591(−69)	8.751(−4)	+1.00057(−74)	9.458(−5)
1.45	−1.78852(−73)	1.458(−3)	−2.53018(−81)	3.474(−4)

$\frac{1}{2}\pi + \omega_+ - \delta$, which is confirmed by the corresponding results. Similarly, when $x = -0.10$ and $x = -1.0$, the corresponding values are $\xi = -0.404$, $\eta = 0$ and $\xi = 0$, $\eta = 0.793$ respectively, so that $\omega_\pm = \frac{1}{2}\pi$ in both cases and the expansion (3.3) is valid in $|\arg\lambda| \leqslant \pi - \delta$.

Table 5: Values of the absolute relative error in $F_3(\lambda;x)$ resulting from the asymptotic expansions (3.3) and (3.4) (with $k \leqslant 2$) for complex λ and real x, with $\lambda = 40e^{i\theta}$, $\varepsilon_1 = 1.20$, $\varepsilon_2 = 2.50$ and $a = \frac{1}{4}$, $b = \frac{1}{2}$, $c = \frac{3}{4}$. Conjugate values are obtained for $\theta < 0$.

$x=0.50$		$x=-0.10$		$x=-1.00$	
$\omega_\pm = 0.228\pi$		$\omega_\pm = \frac{1}{2}\pi$		$\omega_\pm = \frac{1}{2}\pi$	
θ/π	Rel. Error	θ/π	Rel. Error	θ/π	Rel. Error
0	4.666(−6)	0	4.375(−5)	0	2.701(−5)
0.20	4.671(−6)	0.20	4.466(−5)	0.20	3.473(−5)
0.40	4.708(−6)	0.40	4.746(−5)	0.40	3.268(−5)
0.50	4.712(−6)	0.50	4.960(−5)	0.50	3.262(−5)
0.60	4.707(−6)	0.60	5.225(−5)	0.60	3.324(−5)
0.70	4.676(−6)	0.80	5.864(−5)	0.80	3.615(−5)
0.72	8.587(−3)	0.90	6.162(−5)	0.90	1.756(−5)
0.73	1.179(+0)	0.95	4.468(−5)	0.95	7.094(−3)

Finally, in Table 6 we show values of the absolute relative error for complex z, real λ computed from (3.3) and (3.4), and in Table 7 for both z and λ complex computed from (3.3). In this last table, which illustrates the case with $\varepsilon_1 = 1.20$, $\varepsilon_2 = 2.50$, we have selected two values of z situated in the unshaded and shaded regions shown in Fig. 7. The first value of $z = 0.25 + 0.50i$ corresponds to $\xi > 0$, $\eta \neq 0$, whereas the second value of $z = -0.10 + 0.10i$ is situated in the shaded region where $\xi < 0$. The associated values of $\omega_\pm$ are indicated, which are seen to be verified by the numerical results.

Table 6: Values of the absolute relative error in $F_3(\lambda;z)$ resulting from the asymptotic expansions (3.3) and (3.4) (with $k \leqslant 2$) for complex z when $\lambda = 40$ and $a = \frac{1}{4}$, $b = \frac{1}{2}$, $c = \frac{3}{4}$.

$\varepsilon_1 = 1.20,\ \varepsilon_2 = 2.50$		$\varepsilon_1 = 1.20,\ \varepsilon_2 = 2.50$		$\varepsilon_1 = \varepsilon_2 = 1.50$	
z	Rel. Error	z	Rel. Error	z	Rel. Error
0.5	4.666(−6)	-0.1	4.375(−5)	-1.0	2.349(−5)
0.5+0.2i	4.611(−6)	$-0.1+0.2i$	1.407(−6)	$-1.0+0.2i$	2.435(−5)
0.5+0.4i	4.486(−6)	$-0.1+0.4i$	1.354(−6)	$-1.0+0.4i$	1.678(−5)
0.5+0.6i	4.402(−6)	$-0.1+0.6i$	1.332(−6)	$-1.0+0.6i$	1.074(−5)
0.5+0.8i	4.408(−6)	$-0.1+0.8i$	3.760(−7)	$-1.0+0.8i$	7.055(−6)
0.5+1.0i	4.484(−6)	$-0.1+1.0i$	3.606(−7)	$-1.0+1.0i$	4.952(−6)
0.5+2.0i	5.813(−6)	$-0.1+2.0i$	3.627(−7)	$-1.0+2.0i$	2.085(−6)

Table 7: Values of the absolute relative error in $F_3(\lambda;z)$ resulting from the asymptotic expansion (3.3) (with $k \leqslant 2$) when $\varepsilon_1 = 1.20$, $\varepsilon_2 = 2.50$ and $\lambda = 40e^{i\theta}$ for different θ with $a = \frac{1}{4}$, $b = \frac{1}{2}$, $c = \frac{3}{4}$.

$z = 0.25+0.50i$, $\omega_+ = 0.040\pi$, $\omega_- = 0.393\pi$				$z = -0.10+0.10i$, $\omega_\pm = \frac{1}{2}\pi$ $(\xi < 0)$			
θ/π	Rel. Error	θ/π	Rel. Error	θ/π	Rel. Error	θ/π	Rel. Error
0	4.117(−6)			0	3.020(−5)		
0.20	4.131(−6)	−0.20	4.139(−6)	0.20	3.330(−5)	−0.20	2.848(−5)
0.40	4.161(−6)	−0.40	4.173(−6)	0.40	3.715(−5)	−0.40	2.809(−5)
0.50	2.901(−5)	−0.60	4.178(−6)	0.60	3.890(−5)	−0.60	2.884(−5)
0.52	4.986(−3)	−0.80	4.154(−6)	0.80	3.473(−5)	−0.80	3.061(−5)
0.54	7.842(−1)	−0.89	6.661(−2)	0.95	3.974(−3)	−0.95	3.875(−4)

Acknowledgement.
The author wishes to acknowledge the helpful comments made by the referees.

REFERENCES

[1] F. W. J. OLVER, D. W. LOZIER, R. F. BOISVERT AND C. W. CLARK (eds.), *NIST Handbook of Mathematical Functions*, Cambridge University Press, Cambridge, 2010.
[2] R. B. PARIS, *Asymptotics of the Gauss hypergeometric function with large parameters, I*, J. Classical Anal. **2**, 2 (2013), 183–203.
[3] G. N. WATSON, *Asymptotic expansions of hypergeometric functions*, Trans. Cambridge Philos. Soc. **22** (1918), 277–308.

(Received March 15, 2013)

R. B. Paris
School of Computing, Engineering and Applied Mathematics
University of Abertay Dundee
Dundee DD1 1HG, UK